Optik 126 (2015) 6–12

Contents lists available at ScienceDirect

Optik

journal homepage: www.elsevier.de/ijleo

Medical image ensemble registration based on Gaussian mixture model and color component regularization

Shun-bo Hu [a,*], Jeff Orchard [b]

[a] School of Information, Linyi University, Linyi 276005, China
[b] David R. Cheriton School of Computer Science, University of Waterloo, Waterloo, ON, Canada N2L 3G1

ARTICLE INFO

Article history:
Received 12 November 2013
Accepted 16 June 2014

Keywords:
Ensemble registration
Color medical image registration
Gaussian mixture model (GMM)
Color components regularization

ABSTRACT

Ensemble registration has proven to be more robust and accurate than competing pairwise registration methods. Color medical images are commonly applied in medical diagnosis and analysis. In this paper ensemble registration using a Gaussian mixture model is extended from gray images to color medical images. To decrease the transformation differences among color component deformations of the same image, the color component regularization term is incorporated into ensemble registration and a novel total cost function is proposed. Color ensemble registration is implemented to gastroscope images and brain cryosection images. The experimental results show that our color ensemble registration can successfully align color ensemble images with stable color component's transformation.

1. Introduction

Image registration is a common and fundamental operation in image analysis and is used in various areas including remote sensing, medical imaging [1–3], quality control, image segmentation [4], image fusion, and computer vision. During the last decades, many methods for image registration have been developed. However, most of these methods are designed to align only two images at a time in a pairwise fashion.

Some researchers have studied registration of multiple images at the same time – called ensemble registration [5–7] or groupwise registration [8–11]. Ensemble registration based on GMM can avoid calculating high dimensional joint histogram [15], and it will decrease memory and enhance registration speed. Ensemble registration based on GMM can avoid extracting control point [16–18] or other features [19] that will bring extracting error to registration results. Ensemble registration using a Gaussian mixture model (GMM) has been demonstrated for rigid and affine transformations [5] and for non-rigid transformations [6]. However, this method is not used for color image ensemble registration.

In this paper, we present a method that employs clustering to simultaneously align an entire ensemble of medical color images. The main contributions of our method are color components regularization and color components averaging. The color components regularization will make the geometrical transform differences among color components become smaller. The color components averaging can average the geometrical transform of the color components of the same image and eliminate the transform differences among color components.

The rest of this paper is organized as follows. Section 2 describes color ensemble registration and gives the linear solution and implementation framework. Section 3 presents the validation results. Section 4 gives our conclusions.

2. Methods

2.1. Cost function

The total cost function consists of two terms; the first term E_l is the summation of the log-likelihood of red, green and blue components; and the second term E_r is a regularization term used to constrain the spatial deformation of RGB images. This total cost function is defined as

$$E_{\text{total}} = E_l - \lambda E_r \tag{1}$$

where λ is a positive weighting factor.

The first term E_l is defined as the sum of RGB components' cost functions,

$$E_l = E_{lr} + E_{lg} + E_{lb} \tag{2}$$

* Corresponding author.
E-mail addresses: hsbtiger7748@163.com, hushunbo@lyu.edu.cn (S.-b. Hu).

http://dx.doi.org/10.1016/j.ijleo.2014.06.176
0030-4026/

where

$$E_{lr} = \log L_r\left(\phi_r, \theta_r\right) = \sum_x \log p_r\left(I_{rx}^{\theta_r} \middle| \phi_r\right) \tag{3}$$

$$E_{lg} = \log L_g\left(\phi_g, \theta_g\right) = \sum_x \log p_g\left(I_{gx}^{\theta_g} \middle| \phi_g\right) \tag{4}$$

$$E_{lb} = \log L_b\left(\phi_b, \theta_b\right) = \sum_x \log p_b\left(I_{bx}^{\theta_b} \middle| \phi_b\right) \tag{5}$$

The likelihoods $L_r\left(\phi_r, \theta_r\right)$, $L_g\left(\phi_g, \theta_g\right)$ and $L_b\left(\phi_b, \theta_b\right)$ are defined as,

$$L_r\left(\phi_r, \theta_r\right) = \prod_x p_r\left(I_{rx}^{\theta_r} \middle| \phi_r\right) \tag{6}$$

$$L_g\left(\phi_g, \theta_g\right) = \prod_x p_g\left(I_{gx}^{\theta_g} \middle| \phi_g\right) \tag{7}$$

$$L_b\left(\phi_b, \theta_b\right) = \prod_x p_b\left(I_{bx}^{\theta_b} \middle| \phi_b\right) \tag{8}$$

where $I_{rx}^{\theta_r}$, $I_{gx}^{\theta_g}$ and $I_{bx}^{\theta_b}$ are the red, green and blue component of color vector I_x^{θ}, respectively; p_r is a probability function of the red component vector $I_{rx}^{\theta_r}$ for pixel x after applying the spatial transformation with parameters θ_r; ϕ_r is the parameters of the GMM model for the red component. Similarly, p_g and p_b are the probability functions of the green component vector $I_{gx}^{\theta_g}$ and the blue component vector $I_{bx}^{\theta_b}$, respectively.

For color images, the total transformation column vector $\theta = \begin{bmatrix}\theta_1 & \theta_2 & \cdots & \theta_D\end{bmatrix}^T$, where D is the number of color images. The transformation vector of ith color image is $\theta_i = \begin{bmatrix}\theta_{ir}, \theta_{ig}, \theta_{ib}\end{bmatrix}^T$. The red component transformation θ_r is defined as $\theta_r = \begin{bmatrix}\theta_{1r} & \theta_{2r} & \cdots & \theta_{Dr}\end{bmatrix}^T$. Similarly, the green ($\theta_g$) or blue ($\theta_b$) component's transformations are defined with the subscript changing to 'g' or 'b'. If the transformations θ_{ir} have M motion parameters (translation, rotation, etc.), i.e., $\theta_{ir} = \begin{bmatrix}\theta_{ir1} & \theta_{ir2} & \cdots & \theta_{irM}\end{bmatrix}^T$, then the elements' number in column vector θ, θ_i and θ_r is $3MD$, $3M$ and MD, respectively.

The second term is based on the geometrical transformation differences of the RGB components. The energy E_r is defined as

$$\begin{aligned} E_r &= \log E_p \\ &= \log\left(\frac{1}{3}\sum_{i=1}^{D}\left(\left\|\theta_{ir}-\theta_{ig}\right\|^2 + \left\|\theta_{ib}-\theta_{ir}\right\|^2 + \left\|\theta_{ig}-\theta_{ib}\right\|^2\right)\right) \end{aligned} \tag{9}$$

where

$$E_p = \frac{1}{3}\sum_{i=1}^{D}\left(\left\|\theta_{ir}-\theta_{ig}\right\|^2 + \left\|\theta_{ib}-\theta_{ir}\right\|^2 + \left\|\theta_{ig}-\theta_{ib}\right\|^2\right) \tag{10}$$

The parameters θ^* can be obtained by searching the maximal total cost function,

$$\theta^* = \operatorname{argmax}\left(E_{\text{total}}\right) \tag{11}$$

The final transformations $\theta_i^*(1 \le i \le D)$ of ith color image are obtained by averaging their corresponding RGB component transformation,

$$\theta_i^* = \frac{\theta_{ir}^* + \theta_{ig}^* + \theta_{ib}^*}{3} \tag{12}$$

2.2. Gaussian mixture model

The Gaussian mixture model (GMM) is a probabilistic model for density estimation and consists of a mixture of many probability density functions, usually Gaussian, with different means and covariance. The red component is taken as an example, and formulas of the green and blue components are similar. By applying GMM to the joint intensity scatter plot (JISP) of red component, the red clusters in the JISP are modeled as a mixture of K Gaussian functions, each specified by a mean, μ_{rk}, and a covariance matrix, σ_{rk}. Therefore, for a single pixel location x, the likelihood of observing the intensity vector $I_{rx}^{\theta_r}$ is

$$p_r\left(I_{rx}^{\theta_r} \middle| \phi_r\right) = \sum_{k=1}^{K} \pi_{rk} N\left(I_{rx}^{\theta_r}, \mu_{rk}, \sigma_{rk}\right) \tag{13}$$

where the kth Gaussian component is specified by μ_{rk} and σ_{rk}; π_{rk} are the component weights, with $\sum_{k=1}^{K}\pi_{rk} = 1$.

The Gaussian function N denotes the normal distribution,

$$N\left(I_x^{\theta}, \mu, \sigma\right) = \frac{\exp\left(-0.5\left(I_x^{\theta}-\mu\right)^T\sigma^{-1}\left(I_x^{\theta}-\mu\right)\right)}{\sqrt{(2\pi)^D\left|\sigma\right|}} \tag{14}$$

2.3. Optimization

The goal of registration is to maximize the total cost function by appropriate choice of a density estimation of ϕ, i. e., $\phi = \left\{\phi_r, \phi_g, \phi_b\right\}$, $\phi_r = \left\{\pi_{rk}, \mu_{rk}, \sigma_{rk}\right\}$, $\phi_g = \left\{\pi_{gk}, \mu_{gk}, \sigma_{gk}\right\}$, $\phi_b = \left\{\pi_{bk}, \mu_{bk}, \sigma_{bk}\right\}$, and a set of deformation parameters θ. To do this, we alternate two optimization processes, density estimation and motion adjustment.

2.3.1. Density estimation

While holding the motion parameters θ fixed, this process iteratively attempts to improve the density estimate ϕ by using the expectation–maximization (EM) algorithm [12]. The EM algorithm has two steps: expectation and maximization.

The expectation step finds the membership of each intensity vector in the JISP among K clusters. Take the red component as an example. The membership of pixel $I_{rx}^{\theta_r}$ to cluster k is

$$\tau_{rkx} = \frac{\pi_{rk} N\left(I_{rx}^{\theta_r}, \mu_{rk}, \sigma_{rk}\right)}{\sum_k \pi_{rk} N\left(I_{rx}^{\theta_r}, \mu_{rk}, \sigma_{rk}\right)} \tag{15}$$

obviously $\sum_k \tau_{rkx} = 1$.

The maximization step re-estimates the cluster components, μ_{rk}, σ_{rk} and π_{rk}. The new estimated cluster components are given by

$$\hat{\mu}_{rk} = \frac{\sum_x \tau_{rkx} I_{rx}^{\theta_r}}{\sum_x \tau_{rkx}} \tag{16}$$

$$\hat{\sigma}_{rk} = \frac{\sum_x \tau_{rkx}\left(I_{rx}^{\theta_r} - \hat{\mu}_{rk}\right)\left(I_{rx}^{\theta_r} - \hat{\mu}_{rk}\right)^T}{\sum_x \tau_{rkx}} \tag{17}$$

$$\hat{\pi}_{rk} = \frac{\sum_x \tau_{rkx}}{\sum_k \sum_x \tau_{rkx}} \tag{18}$$

2.3.2. Motion adjustment

To optimize the total cost function with respect to the parameters θ, we set its gradient vector to zero.

$$\frac{\partial E_{\text{total}}}{\partial \theta} = \frac{\partial E_l}{\partial \theta} - \lambda\frac{\partial E_r}{\partial \theta} = \frac{\partial E_{lr}}{\partial \theta} + \frac{\partial E_{lg}}{\partial \theta} + \frac{\partial E_{lb}}{\partial \theta} - \lambda\frac{\partial E_r}{\partial \theta} = 0 \tag{19}$$

There are not θ_g and θ_b in the formula of E_{lr}, so $\partial E_{lr}/\partial\theta_g = 0$, $\partial E_{lr}/\partial\theta_b = 0$. Similarly, $\partial E_{lg}/\partial\theta_r = 0$, $\partial E_{lg}/\partial\theta_b = 0$, $\partial E_{lb}/\partial\theta_r = 0$, $\partial E_{lb}/\partial\theta_g = 0$. Therefore,

$$\frac{\partial E_{lr}}{\partial\theta} = \begin{pmatrix} \frac{\partial E_{lr}}{\partial\theta_{1r}} & 0 & 0 & \frac{\partial E_{lr}}{\partial\theta_{2r}} & 0 & 0 & \cdots & \frac{\partial E_{lr}}{\partial\theta_{Dr}} & 0 & 0 \end{pmatrix}^T \tag{20}$$

$$\frac{\partial E_{lg}}{\partial\theta} = \begin{pmatrix} 0 & \frac{\partial E_{lg}}{\partial\theta_{1g}} & 0 & 0 & \frac{\partial E_{lg}}{\partial\theta_{2g}} & 0 & \cdots & 0 & \frac{\partial E_{lg}}{\partial\theta_{Dg}} & 0 \end{pmatrix}^T \tag{21}$$

$$\frac{\partial E_{lb}}{\partial\theta} = \begin{pmatrix} 0 & 0 & \frac{\partial E_{lb}}{\partial\theta_{1b}} & 0 & 0 & \frac{\partial E_{lb}}{\partial\theta_{2b}} & \cdots & 0 & 0 & \frac{\partial E_{lb}}{\partial\theta_{Db}} \end{pmatrix}^T \tag{22}$$

Summing formulas (20)–(22), we obtain,

$$\begin{aligned} \frac{\partial E_l}{\partial\theta} &= \frac{\partial E_{lr}}{\partial\theta} + \frac{\partial E_{lg}}{\partial\theta} + \frac{\partial E_{lb}}{\partial\theta} \\ &= \begin{pmatrix} \frac{\partial E_{lr}}{\partial\theta_{1r}} & \frac{\partial E_{lg}}{\partial\theta_{1g}} & \frac{\partial E_{lb}}{\partial\theta_{1b}} & \frac{\partial E_{lr}}{\partial\theta_{2r}} & \frac{\partial E_{lg}}{\partial\theta_{2g}} & \frac{\partial E_{lb}}{\partial\theta_{2b}} & \cdots & \frac{\partial E_{lr}}{\partial\theta_{Dr}} & \frac{\partial E_{lg}}{\partial\theta_{Dg}} & \frac{\partial E_{lb}}{\partial\theta_{Db}} \end{pmatrix}^T \end{aligned} \tag{23}$$

The first partials of RGB component's cost function ($\partial E_{lr}/\partial\theta_r$, $\partial E_{lg}/\partial\theta_g$, $\partial E_{lb}/\partial\theta_b$) are similarly deduced as in the paper [5],

$$\begin{aligned} \frac{\partial E_{lr}}{\partial\theta_r} &= \begin{pmatrix} \frac{\partial E_{lr}}{\partial\theta_{1r}} & \frac{\partial E_{lr}}{\partial\theta_{2r}} & \cdots & \frac{\partial E_{lr}}{\partial\theta_{Dr}} \end{pmatrix}^T \cong \frac{\partial}{\partial\theta_r}\log L_r\left(\phi_r, \theta_r + \tilde{\theta}_r\right) \\ &= \sum_x \frac{-1}{p_r\left(I_{rx}^{\theta_r}\middle|\phi_r\right)} \sum_{k=1}^{K} \pi_{rk} N\left(I_{rx}^{\theta_r}, \mu_{rk}, \sigma_{rk}\right) \frac{\partial I_{rx}^{\theta_r}}{\partial\theta_r} \sigma_{rk}^{-1}\left(I_{rx}^{\theta_r} + \frac{\partial I_{rx}^{\theta_r}}{\partial\theta_r}^T \tilde{\theta}_r - \mu_{rk}\right) \\ &= \sum_x \frac{-1}{p_r\left(I_{rx}^{\theta_r}\middle|\phi_r\right)} \sum_{k=1}^{K} \pi_{rk} N\left(I_{rx}^{\theta_r}, \mu_{rk}, \sigma_{rk}\right) \frac{\partial I_{rx}^{\theta_r}}{\partial\theta_r} \sigma_{rk}^{-1} \frac{\partial I_{rx}^{\theta_r}}{\partial\theta_r}^T \tilde{\theta}_r + \sum_x \frac{-1}{p_r\left(I_{rx}^{\theta_r}\middle|\phi_r\right)} \sum_{k=1}^{K} \pi_{rk} N\left(I_{rx}^{\theta_r}, \mu_{rk}, \sigma_{rk}\right) \frac{\partial I_{rx}^{\theta_r}}{\partial\theta_r} \sigma_{rk}^{-1}\left(I_{rx}^{\theta_r} - \mu_{rk}\right) \\ &= -A_r\tilde{\theta}_r + b_r \end{aligned} \tag{24}$$

Similarly, we can get

$$\frac{\partial E_{lg}}{\partial\theta_g} = \begin{pmatrix} \frac{\partial E_{lg}}{\partial\theta_{1g}} & \frac{\partial E_{lg}}{\partial\theta_{2g}} & \cdots & \frac{\partial E_{lg}}{\partial\theta_{Dg}} \end{pmatrix}^T \cong -A_g\tilde{\theta}_g + b_g \tag{25}$$

$$\frac{\partial E_{lb}}{\partial\theta_b} = \begin{pmatrix} \frac{\partial E_{lb}}{\partial\theta_{1b}} & \frac{\partial E_{lb}}{\partial\theta_{2b}} & \cdots & \frac{\partial E_{lb}}{\partial\theta_{Db}} \end{pmatrix}^T \cong -A_b\tilde{\theta}_b + b_b \tag{26}$$

where $\tilde{\theta}_r$, $\tilde{\theta}_g$ and $\tilde{\theta}_b$ are a small increment of red, green and blue motion parameters.

Let S be a permutation matrix obtained by applying some row switching to identity matrix, and satisfy

$$S\begin{pmatrix} \frac{\partial E_{lg}}{\partial\theta_g} & \frac{\partial E_{lg}}{\partial\theta_g} & \frac{\partial E_{lg}}{\partial\theta_g} \end{pmatrix}^T = \frac{\partial E_l}{\partial\theta}, \quad S\begin{pmatrix} \tilde{\theta}_r & \tilde{\theta}_g & \tilde{\theta}_b \end{pmatrix}^T = \tilde{\theta} \tag{27}$$

Therefore,

$$\begin{pmatrix} \tilde{\theta}_r & \tilde{\theta}_g & \tilde{\theta}_b \end{pmatrix}^T = S^{-1}\tilde{\theta} \tag{28}$$

Incorporating formulas (24)–(28), we obtain

$$\begin{aligned} \frac{\partial E_l}{\partial\theta} &= S\begin{pmatrix} \frac{\partial E_{lg}}{\partial\theta_g} & \frac{\partial E_{lg}}{\partial\theta_g} & \frac{\partial E_{lg}}{\partial\theta_g} \end{pmatrix}^T \\ &= S\begin{pmatrix} -A_r\tilde{\theta}_r + b_r \\ -A_g\tilde{\theta}_g + b_g \\ -A_b\tilde{\theta}_b + b_b \end{pmatrix} = -S\begin{pmatrix} A_r\tilde{\theta}_r \\ A_g\tilde{\theta}_g \\ A_b\tilde{\theta}_b \end{pmatrix} + S\begin{pmatrix} b_r \\ b_g \\ b_b \end{pmatrix} = -S\begin{pmatrix} A_r & & \\ & A_g & \\ & & A_b \end{pmatrix}\begin{pmatrix} \tilde{\theta}_r \\ \tilde{\theta}_g \\ \tilde{\theta}_b \end{pmatrix} + S\begin{pmatrix} b_r \\ b_g \\ b_b \end{pmatrix} \\ &= -S\begin{pmatrix} A_r & & \\ & A_g & \\ & & A_b \end{pmatrix} S^{-1}\tilde{\theta} + S\begin{pmatrix} b_r \\ b_g \\ b_b \end{pmatrix} \\ &= -A\tilde{\theta} + b \end{aligned} \tag{29}$$

where $A = S \times \operatorname{diag}\begin{pmatrix} A_r & A_g & A_b \end{pmatrix} \times S^{-1}$, $b = S\begin{pmatrix} b_r & b_g & b_b \end{pmatrix}^T$. Note that for permutation matrix, $S^{-1} = S^T$.

Now we consider the second term, the gradient of the regularization E_r. It corresponds to the gradient of log-energy of E_p,

$$\frac{\partial E_r}{\partial\theta} = \frac{\partial}{\partial\theta}\log E_p \tag{30}$$

We replace the log-energy with a nudged version. According to a linear approximation, i.e. $\log E_p^{\theta+\tilde{\theta}} = \log E_p + \left(\partial\log E_p/\partial\theta\right)\tilde{\theta}$. Thus,

$$\begin{aligned} \frac{\partial E_r}{\partial\theta} &= \frac{\partial}{\partial\theta}\log E_p \cong \frac{\partial}{\partial\theta}\log E_p^{\theta+\tilde{\theta}} \\ &= \frac{\partial}{\partial\theta}\log E_p + \frac{\partial^2\log E_p}{\partial\theta^2}\tilde{\theta} \\ &= \frac{1}{E_p}\frac{\partial E_p}{\partial\theta} + \left(\frac{1}{E_p}\frac{\partial^2 E_p}{\partial\theta^2} - \left(\frac{1}{E_p}\frac{\partial E_p}{\partial\theta}\right)\left(\frac{1}{E_p}\frac{\partial E_p}{\partial\theta}\right)^T\right)\tilde{\theta} \end{aligned} \tag{31}$$

From formula (5), the first partial $\partial E_p/\partial\theta$ can be obtained,

$$\frac{\partial E_p}{\partial\theta} = \begin{pmatrix} \frac{\partial E_p}{\partial\theta_{1r}} & \frac{\partial E_p}{\partial\theta_{1g}} & \frac{\partial E_p}{\partial\theta_{1b}} & \cdots \frac{\partial E_p}{\partial\theta_{ir}} & \frac{\partial E_p}{\partial\theta_{ig}} & \frac{\partial E_p}{\partial\theta_{ib}} \cdots \frac{\partial E_p}{\partial\theta_{Dr}} & \frac{\partial E_p}{\partial\theta_{Dg}} & \frac{\partial E_p}{\partial\theta_{Db}} \end{pmatrix}^T \tag{32}$$

where

$$\frac{\partial E_p}{\partial\theta_{ir}} = \frac{1}{3}\left(2\left(\theta_{ir} - \theta_{ig}\right) - 2\left(\theta_{ib} - \theta_{ir}\right)\right) = \frac{2}{3}\left(2\theta_{ir} - \theta_{ib} - \theta_{ig}\right) \tag{33}$$

$$\frac{\partial E_p}{\partial\theta_{ig}} = \frac{2}{3}\left(2\theta_{ig} - \theta_{ib} - \theta_{ir}\right) \tag{34}$$

$$\frac{\partial E_p}{\partial\theta_{ib}} = \frac{2}{3}\left(2\theta_{ib} - \theta_{ig} - \theta_{ir}\right) \tag{35}$$

The second partial $\left(\partial^2 E_p/\partial\theta^2\right)$ is

$$\frac{\partial^2 E_p}{\partial\theta^2} = \frac{2}{3}U \tag{36}$$

where U is a constant block diagonal matrix.

$$U = \operatorname{diag}\begin{pmatrix} U_1 & U_2 & \cdots & U_D \end{pmatrix} \tag{37}$$

U_i is a Toeplitz matrix with the size of $3M \times 3M$,

$$U_i = \text{toep}\left(2 \quad 0 \quad \cdots \quad 0 \quad -1 \quad 0 \quad \cdots 0 \quad -1\ 0 \quad \cdots \quad 0\right) \tag{38}$$

In the above formula, the number of zeros between non-zeros is $M-1$.

Combining the two terms, $\partial E_l/\partial\theta$ and $\partial E_r/\partial\theta$, the gradient of the total cost function becomes

$$\begin{aligned}\frac{\partial E_{\text{total}}}{\partial\theta} &= \frac{\partial E_l}{\partial\theta} - \lambda\frac{\partial E_r}{\partial\theta} \\ &\cong \left(-A\tilde{\theta}+b\right) - \lambda\left(\frac{1}{E_p}\frac{\partial E_p}{\partial\theta} + \left(\frac{4}{3E_p}E - \left(\frac{1}{E_p}\frac{\partial E_p}{\partial\theta}\right)\left(\frac{1}{E_p}\frac{\partial E_p}{\partial\theta}\right)^T\right)\tilde{\theta}\right) = 0\end{aligned} \tag{39}$$

After expanding the brackets and reorganizing the remaining terms, we get the linear system

$$\left(A + \lambda\left(\frac{4}{3E_p}E - \left(\frac{1}{E_p}\frac{\partial E_p}{\partial\theta}\right)\left(\frac{1}{E_p}\frac{\partial E_p}{\partial\theta}\right)^T\right)\right)\tilde{\theta} = b - \lambda\left(\frac{1}{E_p}\frac{\partial E_p}{\partial\theta}\right), \tag{40}$$

or more concisely,

$$(A+\lambda G)\tilde{\theta} = b - \lambda\left(\frac{1}{E_p}\frac{\partial E_p}{\partial\theta}\right), \quad W\tilde{\theta} = q \tag{41}$$

where $G = \left(4/3E_p\right)E - \left(\left(1/E_p\right)\left(\partial E_p/\partial\theta\right)\right)\left(\left(1/E_p\right)\left(\partial E_p/\partial\theta\right)\right)^T$, $A+\lambda G = W$ and $q = b - \lambda\left(\left(1/E_p\right)\left(\partial E_p/\partial\theta\right)\right)$. Solving the linear system for $\tilde{\theta}$ gives the optimal increment of deformation parameters. According to the linear approximations, the increment is used to adjust the current estimate for θ.

By formula (41), we obtain

$$\tilde{\theta} = W^{-1}q \tag{42}$$

$\tilde{\theta}$ is used to renew the geometrical transformation,

$$\theta_{\text{new}} = \theta_{\text{old}} + \tilde{\theta} \tag{43}$$

Two operation of density estimation and motion adjustment will repeat until $\tilde{\theta}$ is smaller than a value or until the numbers of iterations reaches a predetermined maximum.

2.4. Implementation

We implemented our method in Matlab (Mathworks Inc., Natick, Massachusetts). **Algorithm 1** summarizes the code for our method.

Algorithm 1 Color ensemble registration

input: initial color ensemble I_0 : $\left\{ I_{0\_r} \quad I_{0\_g} \quad I_{0\_b} \right\}$
input: initial motion parameters θ : $\left\{ \theta_r \quad \theta_g \quad \theta_b \right\}$
input: initial GMM parameters ϕ : $\left\{ \phi_r \quad \phi_g \quad \phi_b \right\}$
for each scales **do**
  I_{scaled} : $\left\{ I_{scaled\_r} \quad I_{scaled\_g} \quad I_{scaled\_b} \right\}$ ← scale color ensemble I_0
  I_r ← apply motion (θ_r) to red ensemble I_{scaled_r}
  I_g ← apply motion (θ_g) to green ensemble I_{scaled_g}
  I_b ← apply motion (θ_b) to blue ensemble I_{scaled_b}
Repeat
  for K_1 iterations **do**
    ϕ : $\left\{ \phi_r \quad \phi_g \quad \phi_b \right\}$ ← EM step (see Formulas (15)–(18))
  end for
  for K_2 iterations **do**
    $\tilde{\theta}$ ← motion adjustment (see Formula (42))
    $\tilde{\theta} \leftarrow \theta + \tilde{\theta}$
    $\left\{ \theta_r \quad \theta_g \quad \theta_b \right\} \leftarrow \tilde{\theta}$
    I_r ← apply motion (θ_r) to red ensemble I_{scaled_r}
    I_g ← apply motion (θ_g) to green ensemble I_{scaled_g}
    I_b ← apply motion (θ_b) to blue ensemble I_{scaled_b}
  end for
  until converged ($\tilde{\theta}$ is small)
end for
  θ ← average of color components' transformation (see Formula (12))
  I ← apply motion (θ) to ensemble I_{scaled}
output: I is aligned color ensemble at full scale
output: θ holds the optimal motion parameters
output: ϕ holds the GMM parameters

Each color image in the ensemble is subject to the same type of geometrical transformation, and has the same number of parameters. Thus, the number of motion parameters stored in the vector of θ_r, θ_g and θ_b is MD, and the number stored in the vector of θ is $3MD$.

3. Experiments and discussion

Experiments are conducted to study the color image ensemble registration performances. Section 3.1 aligns color gastroscope images. Section 3.2 aligns color brain cryosection images. A multiresolution framework is used. The solution at each scale is taken as an initial guess for the next scale. Color images are registered at scales 10%, 20%, 50%, and then finally 100%. The weighting factor in Formula (1) is set to one. Computing environment is as following: Intel Core i7 CPU 2.7 GHz, 16G memory, OS X 10.8.4, and Matlab 2013a.

3.1. Color gastroscope image registration

The first dataset is gastroscope images that come from Linyi people's hospital. In Fig. 1(a)–(c) are original input images where (b) and (c) are rotated versions of (a). Fig. 1(d) is the average of three original input images. Fig. 1(e) is a mask image with the same size as the input image. Fig. 1(f) is the average of the aligned results of (a)–(c). Fig. 1(g) is three-dimensional JISP of red components in the original input images before registration. Fig. 1(h) is three-dimensional JISP of red components in the aligned color images and corresponding Gaussian components for the 3-D registration test. Fig. 1(i) is the difference image between (a) and (f). The clusters in Fig. 1(h) are more focused than Fig. 1(g). This implies that our color ensemble registration method gets good organ correspondences. It is seen that Fig. 1(f) is clearer than (d) especially in the area of blood vessels and in the ROI (region of interest) of (i) the differences are negligible. This implies that the results using our color images ensemble method are good.Quantitative analysis is used to compare the performances of three ensemble registration methods. These three methods are named as M1, M2 and M3, respectively; where M1: Converting D color images to gray images (e.g. rgb2gray

Table 1
Mean error (standard deviation) between gold standard transformations and estimated transformations under color gastroscope images registration.

Parameters		M1	M2	M3
The second image in ensemble	Rotation degrees	-2.15×10^{-3} ($\pm4.11\times10^{-3}$)	-8.69×10^{-4} ($\pm3.58\times10^{-3}$)	$\mathbf{5.89\times10^{-4}}$ ($\mathbf{\pm3.12\times10^{-3}}$)
	x Translation pixels	8.58×10^{-3} ($\pm7.62\times10^{-3}$)	$\mathbf{-3.75\times10^{-3}}$ ($\pm8.24\times10^{-3}$)	6.02×10^{-3} ($\mathbf{\pm7.07\times10^{-3}}$)
	y Translation pixels	2.62×10^{-2} ($\pm1.52\times10^{-2}$)	$\mathbf{3.58\times10^{-3}}$ ($\mathbf{\pm4.93\times10^{-3}}$)	1.92×10^{-2} ($\pm1.24\times10^{-2}$)
The third image in ensemble	Rotation degrees	-2.53×10^{-3} ($\pm2.99\times10^{-3}$)	-1.12×10^{-3} ($\pm3.21\times10^{-3}$)	$\mathbf{6.95\times10^{-4}}$ ($\mathbf{\pm1.70\times10^{-3}}$)
	x Translation pixels	1.01×10^{-2} ($\pm6.25\times10^{-3}$)	-3.73×10^{-3} ($\pm8.13\times10^{-3}$)	$\mathbf{3.08\times10^{-3}}$ ($\mathbf{\pm7.32\times10^{-3}}$)
	y Translation pixels	2.19×10^{-2} ($\pm1.57\times10^{-2}$)	$\mathbf{4.29\times10^{-3}}$ ($\mathbf{\pm5.24\times10^{-3}}$)	5.34×10^{-3} ($\pm9.78\times10^{-3}$)

Table 2
Mean (standard deviation) of the transformation differences among RGB components of the same color gastroscope images.

Parameters		G-R		B–R	
		M2	M3	M2	M3
The second image in ensemble	Rotation degrees	6.64×10^{-3} ($\pm4.52\times10^{-3}$)	$\mathbf{-3.79\times10^{-3}}$ ($\mathbf{\pm2.03\times10^{-3}}$)	6.41×10^{-3} ($\pm7.83\times10^{-3}$)	$\mathbf{-2.07\times10^{-3}}$ ($\mathbf{\pm2.63\times10^{-3}}$)
	x Translation pixels	-1.65×10^{-3} ($\pm6.48\times10^{-3}$)	$\mathbf{-1.59\times10^{-3}}$ ($\mathbf{\pm1.53\times10^{-3}}$)	-9.41×10^{-3} ($\pm9.68\times10^{-3}$)	$\mathbf{-7.9\times10^{-3}}$ ($\mathbf{\pm6.01\times10^{-3}}$)
	y Translation pixels	-1.84×10^{-2} ($\pm9.68\times10^{-3}$)	$\mathbf{-9.24\times10^{-4}}$ ($\mathbf{\pm1.74\times10^{-3}}$)	-3.47×10^{-2} ($\pm3.28\times10^{-2}$)	$\mathbf{-1.84\times10^{-2}}$ ($\mathbf{\pm1.37\times10^{-2}}$)
The third image in ensemble	Rotation degrees	6.72×10^{-3} ($\pm4.67\times10^{-3}$)	$\mathbf{-3.88\times10^{-3}}$ ($\mathbf{\pm2.18\times10^{-3}}$)	6.77×10^{-3} ($\pm7.98\times10^{-3}$)	$\mathbf{-1.66\times10^{-3}}$ ($\mathbf{\pm2.11\times10^{-3}}$)
	x Translation pixels	-3.38×10^{-3} ($\pm5.47\times10^{-3}$)	$\mathbf{-1.94\times10^{-3}}$ ($\mathbf{\pm1.55\times10^{-3}}$)	-1.11×10^{-2} ($\pm1.02\times10^{-2}$)	$\mathbf{-6.17\times10^{-3}}$ ($\mathbf{\pm6.28\times10^{-3}}$)
	y Translation pixels	-1.51×10^{-2} ($\pm9.58\times10^{-3}$)	$\mathbf{-9.66\times10^{-4}}$ ($\mathbf{\pm1.69\times10^{-3}}$)	-2.34×10^{-2} ($\pm3.2\times10^{-2}$)	$\mathbf{-2\times10^{-2}}$ ($\mathbf{\pm1.62\times10^{-2}}$)

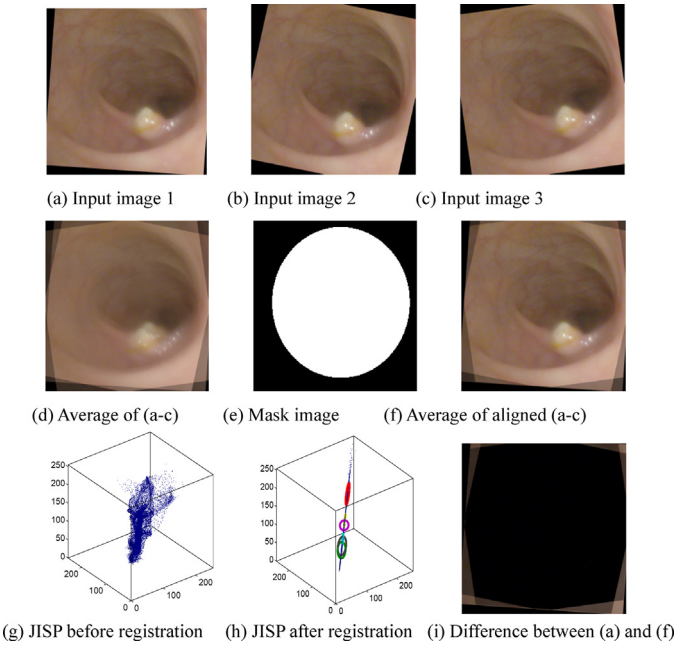

Fig. 1. Registration of color gastroscope images.

function), and then applying gray ensemble registration method [5] to these D gray images; M2: taking each color component as a gray image, and then applying gray ensemble registration method [5] to these 3D gray images; M3: our color ensemble registration method.

Fifty trial ensembles are generated by applying randomly generated rigid-body displacements to color gastroscope images, chosen uniformly from the range [−3,3] pixels translation or [−1010] degrees rotation. The performance of each registration method is gauged by comparing the estimated transformations to the true standard transformations. These differences are calculated between the estimated displacements and the corresponding true displacements. The first input image is used as a reference image, and the other images are used as floating images. The means and standard deviations of these differences using three registration methods are shown in Table 1. The means (standard deviations) of the transformation differences among red, green and blue components of the same color images before color components average are shown in Table 2, e.g. 'G–R' denotes red transformation subtracts green transformation. From Table 1 we can see that M3 method is more accurate than M1 method in all parameters and M2 method in rotation and some translation parameters. Even though in some translation parameter M3 are less accurate than M2 method, from Table 2 it is seen that the transformation differences among red, green and blue components using M3 method are smaller than those corresponding differences using M2 method. These imply that our color ensemble registration method can obtain accurate registration results with stable color component's transformation.

3.2. Color brain cryosection image registration

The second dataset is brain cryosection images that come from the Visible Human Project [13,14]. In Fig. 2(a)–(c), are original input images. (b) and (c) are rotated versions of (a). Fig. 2(d) is a mask image with the same size as input image. Fig. 2(e) is the average of three original input images. Fig. 2(f) is the average of the aligned results of (a)–(c). Fig. 2(g) is the three-dimensional JISP of red components in the original input images before registration. Fig. 2(h) is three-dimensional JISP of red components in the aligned color images and corresponding Gaussian components for the 3-D

Table 3
Mean error (standard deviation) between gold standard transformations and estimated transformations under brain cryosection images registration.

Parameters		M1	M2	M3
The second image in ensemble	Rotation degrees	-1.99×10^{-4} ($\pm1.83\times10^{-3}$)	-2.77×10^{-3} ($\pm1.78\times10^{-3}$)	$\mathbf{-6.02\times10^{-5}}$ ($\mathbf{\pm1.71\times10^{-3}}$)
	x Translation pixels	3.07×10^{-4} ($\pm1.51\times10^{-2}$)	3.06×10^{-3} ($\mathbf{\pm1.47\times10^{-2}}$)	$\mathbf{5.42\times10^{-5}}$ ($\pm1.49\times10^{-2}$)
	y Translation pixels	-2.39×10^{-3} ($\pm1.63\times10^{-2}$)	-3.31×10^{-3} ($\mathbf{\pm1.61\times10^{-2}}$)	$\mathbf{-2.12\times10^{-3}}$ ($\pm1.69\times10^{-2}$)
The third image in ensemble	Rotation degrees	-1.78×10^{-4} ($\pm9.25\times10^{-4}$)	-2.65×10^{-3} ($\pm9.36\times10^{-4}$)	$\mathbf{2.71\times10^{-5}}$ ($\mathbf{\pm9.12\times10^{-4}}$)
	x Translation pixels	$\mathbf{-7.12\times10^{-4}}$ ($\pm1.45\times10^{-2}$)	2.26×10^{-3} ($\pm1.40\times10^{-2}$)	-8.59×10^{-4} ($\mathbf{\pm1.39\times10^{-2}}$)
	y Translation pixels	1.48×10^{-3} ($\pm1.71\times10^{-2}$)	$\mathbf{8.92\times10^{-4}}$ ($\mathbf{\pm1.65\times10^{-2}}$)	1.43×10^{-3} ($\pm1.70\times10^{-2}$)

Table 4
Mean (standard deviation) of the transformation differences among RGB components of the same color brain cryosection images.

Parameters		G–R		B–R	
		M2	M3	M2	M3
The second image in ensemble	Rotation degrees	-2.26×10^{-3} ($\pm4.04\times10^{-4}$)	$\mathbf{-4.12\times10^{-4}}$ ($\mathbf{\pm4.03\times10^{-4}}$)	-4.72×10^{-3} ($\pm1.05\times10^{-3}$)	$\mathbf{-5.65\times10^{-4}}$ ($\mathbf{\pm1.02\times10^{-3}}$)
	x Translation pixels	1.15×10^{-2} ($\pm5.83\times10^{-3}$)	$\mathbf{5.98\times10^{-4}}$ ($\mathbf{\pm2.69\times10^{-3}}$)	-2.36×10^{-3} ($\pm7.76\times10^{-3}$)	$\mathbf{-2.91\times10^{-4}}$ ($\mathbf{\pm7.71\times10^{-3}}$)
	y Translation pixels	5.37×10^{-3} ($\pm3.41\times10^{-3}$)	$\mathbf{-1.13\times10^{-3}}$ ($\mathbf{\pm2.87\times10^{-3}}$)	-1.04×10^{-2} ($\pm1\times10^{-2}$)	$\mathbf{-3.49\times10^{-3}}$ ($\mathbf{\pm9.77\times10^{-3}}$)
The third image in ensemble	Rotation degrees	-2.11×10^{-3} ($\pm5.08\times10^{-4}$)	$\mathbf{-2.96\times10^{-4}}$ ($\mathbf{\pm3.32\times10^{-4}}$)	-4.23×10^{-3} ($\pm5.17\times10^{-4}$)	$\mathbf{-1.32\times10^{-4}}$ ($\mathbf{\pm5.15\times10^{-4}}$)
	x Translation pixels	1.17×10^{-2} ($\pm6.24\times10^{-3}$)	$\mathbf{4.07\times10^{-4}}$ ($\mathbf{\pm2.48\times10^{-3}}$)	-1.89×10^{-3} ($\pm2.72\times10^{-3}$)	$\mathbf{3.29\times10^{-5}}$ ($\pm2.99\times10^{-3}$)
	y Translation pixels	5.46×10^{-3} ($\pm3.11\times10^{-3}$)	$\mathbf{-1.97\times10^{-4}}$ ($\mathbf{\pm2.62\times10^{-3}}$)	-7.04×10^{-3} ($\pm4.46\times10^{-3}$)	$\mathbf{6.42\times10^{-5}}$ ($\mathbf{\pm4.15\times10^{-3}}$)

Fig. 2. Registration of color brain cryosection images.

registration test. The clusters in Fig. 2(h) are more focused than Fig. 2(g). This implies that our color ensemble registration method offers good organ correspondences. It is seen that Fig. 2(f) is clearer than (e), which shows that our color image ensemble registration method is working.

Fifty trial ensembles are generated by applying randomly generated rigid-body displacements, which are chosen uniformly from the range [−4,4] pixels translation or [−1010] degrees rotation. The first input image is used as a reference image, and the other newly generated images are used as floating images. The means and standard deviations of these differences are compared in Table 3. The means (standard deviations) of the transformation differences among RGB components of the same color images before color components average are shown in Table 4. From Table 3 we can see that M3 method is more accurate than M1 method in most of parameters and more accurate than M2 method in rotation and some translation parameters. Even though in some translation parameter M3 are less accurate than M2 method, from Table 4 it is seen that most of transformation differences among red, green and blue components using M3 method are smaller than those corresponding differences using M2 method. These imply that our color ensemble registration method can obtain accurate registration results with more stable color component's transformation.

4. Conclusions

This paper applies the ensemble registration method to align simultaneously the ensembles of medical color images. We reformulate the cost function and the optimization processes of the ensemble registration method with a color regularization term based on mean absolute difference of color component deformations. A multi- resolution framework is used to optimize the total cost function. At last the optimal parameters are averaged by their RGB color components' transformation. The ensemble registration experiments of two color image sets are performed. The experimental results show that our ensemble registration method with color component regularization can be successfully applied to ensemble registration of medical color images. Our color ensemble registration method can generally obtain more accurate registration results in contrast to traditional gray ensemble registration methods, and can get more stable color component's transformation.

Acknowledgments

This work was supported by National Natural Science Foundation of China (61102040 and 31000744), China Scholarship Council, and the Preeminent Youth Fund of Linyi University (4313104).

References

[1] H.C. Hendargo, R. Estrada, S.J. Chiu, C. Tomasi, S. Farsiu, J.A. Izatt, Automated non-rigid registration and mosaicing for robust imaging of distinct retinal capillary beds using speckle variance optical coherence tomography, Biomed. Opt. Express 4 (6) (2013) 803–821.

[2] Y.M. Liew, R.A. McLaughlin, F.M. Wood, D.D. Sampson, Motion correction of in vivo three-dimensional optical coherence tomography of human skin using a fiducial marker, Biomed. Opt. Express 3 (8) (2012) 1774–1786.

[3] I.V. Larina, K.V. Larin, M.E. Dickinson, M. Liebling, Sequential Turning Acquisition and Reconstruction (STAR) method for four-dimensional imaging of cyclically moving structures, Biomed. Opt. Express 3 (3) (2012) 650–660.

[4] V. Kajić, M. Esmaeelpour, B. Považay, D. Marshall, P.L. Rosin, W. Drexler, Automated three-dimensional choroidal vessel segmentation of 3D 1060 nm OCT retinal data, Biomed. Opt. Express 4 (1) (2013) 134–150.

[5] J. Orchard, R. Mann, Registering a multisensor ensemble of images, IEEE Trans. Med. Imaging 19 (5) (2010) 1236–1247.

[6] H.Y. Kim, J. Orchard, Registering a non-rigid multi-sensor ensemble of images, in: Engineering in Medicine and Biology Society-EMBC, IEEE, New York, NY, 2010, pp. 5935–5938.

[7] Z. Spiclin, B. Likar, F. Pernus, Groupwise registration of multimodal images by an efficient joint entropy minimization scheme, IEEE Trans. Image Process. 21 (5) (2012) 2546–2558.

[8] G. Wu, Q. Wang, H. Jia, D. Shen, Feature-ased groupwise registration by hierarchical anatomical correspondence detection, Human Brain Mapp. 33 (2) (2012) 253–271.

[9] H. Lombaert, L. Grady, X. Pennec, J.M. Peyrat, N. Ayache, F. Cheriet, Groupwise spectral log-demons framework for atlas construction, in: Medical Computer Vision. Recognition Techniques and Applications in Medical Imaging, Springer, Berlin Heidelberg, 2013, pp. 11–19.

[10] C.J. Twining, T. Cootes, S. Marsland, V. Petrovic, R. Schestowitz, C.J. Taylor, A unified information–theoretic approach to groupwise non-rigid registration and model building. Information Processing in Medical Imaging, Springer, Berlin Heidelberg, 2005, pp. 1–14.

[11] G. Wu, H. Jia, Q. Wang, D. Shen, SharpMean: Groupwise registration guided by sharp mean image and tree-based registration, NeuroImage 56 (4) (2011) 1968–1981.

[12] G.J. McLachlan, K.E. Basford, Mixture models, in: Inference and Applications to Clustering, Marcel Dekker, New York, NY, 1988.

[13] M.J. Ackerman, The visible human project, Proceedings of the IEEE 86 (3) (1998) 504–511.

[14] Brain cryosection images from the Visible Human Project, Online available at: http://www.nlm.nih.gov/research/visible/photos.html (retrieved October 31, 2014).

[15] J. Zhang, A. Rangarajan, Multimodality image registration using an extensible information metric and high dimensional histogramming, in: Information Processing in Medical Imaging, Springer, Berlin Heidelberg, 2005, pp. 725–737.

[16] G. Wu, Q. Wang, H. Jia, et al., Feature-based groupwise registration by hierarchical anatomical correspondence detection, Human Brain Mapp. 33 (2) (2012) 253–271.

[17] D. Lowe, Distinctive image features from scale-invariant key points, Int. J. Comput. Vis. 60 (2) (2004) 91–110.

[18] K. Mikolajczyk, C. Schmid, Scale and affine invariant interest point detectors, Int. J. Comput. Vis. 60 (1) (2004) 63–86.

[19] Y. Saeys, I. Inza, P. Larrañaga, A review of feature selection techniques in bioinformatics, Bioinformatics 23 (19) (2007) 2507–2517.